Micromechanical Processes and Failure Phenomena in Reactively Compatibilized Blends of Polyamide 6 and Styrenic Polymers. II. Polyamide 6/Styrene-Acrylonitrile Copolymer Blends

U. A. Handge,[1] C. Sailer,[2]* H. Steininger,[3] M. Weber,[4] St. Scholtyssek,[5] V. Seydewitz,[5] G. H. Michler[5]

[1]*Department of Polymer Engineering, University of Bayreuth, D-95447 Bayreuth, Germany*
[2]*Department of Materials, Institute of Polymers, ETH Zurich CH-8093, Switzerland*
[3]*BASF SE, Polymer Research, GKP/E, D-67056 Ludwigshafen am Rhein, Germany*
[4]*BASF SE, Polymer Research, GKT/B, D-67056 Ludwigshafen am Rhein, Germany*
[5]*Faculty of Engineering Science, Institute of Physics, Martin-Luther-University Halle-Wittenberg, D-06099 Halle/S, Germany*

Received 21 May 2009; accepted 27 July 2009
DOI 10.1002/app.31270
Published online 15 October 2009 in Wiley InterScience (www.interscience.wiley.com).

ABSTRACT: This work reports on morphological, mechanical, and micromechanical properties of polyamide 6 (PA 6), a styrene-acrylonitrile copolymer (SAN), and their blends, which were reactively compatibilized using a styrene-acrylonitrile maleic anhydride (SANMA) terpolymer. Transmission electron microscopy (TEM) investigations revealed the phase morphology of the blends, which is characterized by inclusions of the minor component in the matrix of the major phase. The blend with 50% PA 6 and 50% SAN depicted a cocontinuous morphology. Using a microtensile device for TEM, the samples were deformed under uniaxial loading in the "dry" state (characterized by a zero water content in the PA 6 phase) and in a "wet" state (with water in the PA 6 phase). Whereas the dry blends behaved brittle, the wet blends showed a larger ductility with the formation of deformation bands in the matrix (PA 6 or SAN), which were initiated by stress concentration at the SAN and PA 6 particles, respectively. In the interface of blends with a PA 6 matrix and SAN inclusions, two phenomena were observed: partial cavitation and debonding on the one hand and partial fibrillation on the other hand. J Appl Polym Sci 115: 2529–2539, 2010

Key words: reactive compatibilization; polymer blends; micromechanics; PA 6; SAN

INTRODUCTION

The morphological, mechanical, and rheological properties of polymer blends have been the focus of intensive research activities since many decades.[1,2] Reactive compatibilization is a technologically widely applied procedure to enhance the mechanical properties of blends of immiscible or incompatible polymers.[3–5] To deepen the understanding of structure–property relations, a series of investigations has been carried out on the mechanical and rheological properties of reactively compatibilized blends. This study focuses on commercially relevant blends of polyamide 6 (PA 6) and styrenic polymers. Its aim is to investigate the micromechanical deformation mechanisms during tensile deformation. The work is split into two parts. The first part is devoted to blends of PA 6 and an acrylonitrile-butadiene-styrene (ABS) copolymer.[6] Tensile tests were performed on thin sections of the blends within a transmission electron microscope (TEM). Micromechanical tests on blends of PA 6 and a styrene-acrylonitrile copolymer (SAN) are targeted in this article (Part II of the investigations). SAN and ABS are distinguished by their butadiene content which is 0 and 10 wt %, respectively. Thus, comparison of the properties of the two series of blends PA 6/SAN and PA 6/ABS, respectively, should yield the impact of rubber particles on the micromechanical behavior. The mechanical investigations were coordinated by the IUPAC Subcommittee "Structure and Properties of Commercial Polymers" (IUPAC project no. 2005-023-2-400).

In the earlier works, the thermal and morphological properties of blends of (PA 6) with styrenic

Present address: Trüb AG, CH-5001 Aarau, Switzerland.
Correspondence to: U. A. Handge (ulrich.handge@uni-bayreuth.de).

Contract grant sponsor: Swiss National Science Foundation (to C. S. and U. A. H.); contract grant number: 200021-103287.

Contract grant sponsor: International Union of Pure and Applied Chemistry (to chairman H. ST.); contract grant number: 2005-023-2-400.

TABLE I
Physical Properties and Composition of Reactively Compatibilized Blends of PA 6 and SAN

Physical properties of the polyamide 6 (PA 6) and the styrene-acrylonitrile copolymer (SAN) of this study. The SAN grade contained a constant amount of 6.8 wt % of SANMA

	T_g(°C)	T_m(°C)	M_n(g/mol)	M_w(g/mol)	M_w/M_n	η_0 at 240°C (Pas)
PA 6	53	221	23,000	121,000	5.3	8400
SAN	109	–	57,800	150,000	2.6	2400

Composition of reactively compatibilized blends of PA 6 and SAN

	PA 6 (wt %)	SAN (wt %)	SANMA (wt %)
PA 6	100.0	0.0	0.0
70% PA 6/30% SAN	70.0	28.0	2.0
50% PA 6/50% SAN	50.0	46.6	3.4
30% PA 6/70% SAN	30.0	65.2	4.8
SAN	0.0	93.2	6.8

polymers were discussed by Jafari et al.[7,8] These studies revealed that the concentration of compatibilizer strongly affects the microstructure (disperse or cocontinuous morphology) and in addition the crystallization rate of the blend. Lee et al.[9] investigated the morphology of compatibilized PA 6/ABS blends as a function of composition, compatibilizer concentration, and feed rate during extrusion. The mean size of the dispersed domains attained a saturation minimum at a compatibilizer content of 15 wt %. In the work of Pötschke and Paul,[10] the development of cocontinuous structures in PA 6/SAN blends was investigated making use of various techniques.

A series of investigations on morphological and mechanical properties was performed by Paul and coworkers. In Ref. [11], the influence of the functional group of the compatibilizing agent and the amount of functional groups per chain was studied for PA 6/SAN blends. For Majumdar et al.,[12] the evolution of the morphology during reactive compatibilization of PA 6/SAN blends with a PA 6 matrix along the screw of the extrusion device was in focus. Transmission electron microscope investigations of PA 6/ABS specimens, which failed in a double-notch four-point bending geometry, showed that cavitation of rubber particles and subsequent shear yielding of the PA 6 matrix increases the toughness of the blends.[13] Results of mechanical tests indicated that the lowest ductile to brittle transition temperature is associated with blends whose ABS domains are most efficiently dispersed.[14] A systematic study of the properties of these PA 6/ABS blends revealed that rubber particles with a monodisperse size distribution and a low-melt viscosity lead to a larger low-temperature toughness than rubber particles with a broader distribution and higher viscosity.[15] Tensile properties of reactively compatibilized blends were also investigated in Ref. [16]. This work elucidated that under tensile loading SAN particles of compatibilized blends become elongated and undergo shear yielding. The effect of compatibilizer concentration on the ductile-brittle transition was studied by Araújo et al.[17] Blends compatibilized with maleate copolymers exhibit the lowest ductile-brittle transition temperature. Finally, several investigations based upon rotational and extensional rheometry, demonstrated the impact of reactive compatibilization on rheological properties of PA 6/SAN blends with different types of morphology and varying concentration of compatibilizer.[18–21] In summary, various methods to compatibilize blends of PA 6 and styrenic polymers were investigated and their influence on the macroscopic properties was discussed.

In this study, we report on the mechanical properties of reactively compatibilized PA 6/SAN and PA 6/ABS blends. In the preceeding Part I, where blends of PA 6 and ABS were studied, it was shown that the phase morphology determined the mechanical properties. Whilst rubber particles did not play the decisive role for the PA 6/ABS blends, they play in neat ABS. Part II of these investigations is subjected to PA 6/SAN blends. The objective was to analyze the micromechanical mechanisms which control tensile deformation. Therefore, micromechanical tests were performed using semithin sections within a transmission electron microscope. Analogous to Part I, blends with a disperse and a cocontinuous morphology were investigated at two different moisture contents of PA 6, called dry and wet, respectively.

EXPERIMENTAL

Materials

The components of the blends were polyamide 6 (PA 6, Ultramid® B40) and a SAN both provided by BASF SE (Ludwigshafen am Rhein, Germany).

TABLE II
Mean Values of Tensile Test Data: Young's Modulus *E*, Maximum Stress σ_{max}, Yield Stress σ_{yield}, and Strain at Break ε_{break} of PA 6, SAN, and PA 6/SAN Blends

	E (MPa)	Max. stress σ_{max} (M)/yield stress σ_{yield} (Y) (MPa)	Elongation at break ε_{break}(%)	Fracture mechanism
PA 6	3220	80 (M)/76 (Y)	230.0	Ductile
70% PA 6/30% SAN	3360	78 (M)	3.7	Brittle
50% PA 6/50% SAN	3560	76 (M)	2.4	Brittle
30% PA 6/70% SAN	3730	74 (M)	2.2	Brittle
SAN	3840	77 (M)	2.3	Brittle

Table I summarizes some physical properties of the blend components and the blend compositions. Styrene-acrylonitrile-maleic anhydride (SANMA), a random terpolymer which served as compatibilizer was added to the SAN grade at a fraction of SANMA of 6.8 wt %. The terpolymer was composed of 2 wt % maleic anhydride, 29 wt % acrylonitrile, and 69 wt % styrene. The weight average of the molecular weight M_w of SANMA was 115,000 g/mol and the number average M_n was 52,000 g/mol. At an average, 20 maleic anhydride groups were randomly distributed along each chain of SANMA.

In this study, three PA 6/SAN blends were prepared by melt extrusion. After premixing of granules of the blend components and drying under vacuum conditions at $T = 80°C$ for 7 days, blending was performed on a corotating twin screw extruder at $T = 240°C$ (Brabender, Duisburg, Germany). The diameter of the screws was 25 mm with a *L/D* ratio of 22. The screw rotation speed was 50 $min^{-1.}$ Weight concentrations ϕ of PA 6 in the blends were 30, 50, and 70%, respectively (cf. Table II). To compare the properties of the neat components with those of the blends, the neat materials were extruded under the same conditions as the blends. The extrudate was piled up to compact objects of roughly 250 g mass. After solidification, these extruded specimens were cut into pieces with parallel surfaces and subsequently compression-molded under vacuum into plates of dimensions $4 \times 130 \times 150$ mm^3. Molding temperature and time were $T = 240°C$ and 30 min, repectively. Samples for the mechanical testing were milled out of the compression-molded plates.

During melt mixing of the blend constituents, maleic anhydride groups of SANMA react with amino end groups of PA 6. This reaction leads to the formation of SAN-*graft*-PA 6 copolymers (Fig. 1). The graft-copolymers are preferentially located at the interfaces between PA 6 and SAN phases. As these molecules contain two types of segments, which fit either into PA 6 or SAN, they convey compatibilization of the two phases and enhance the interfacial adhesion. The concentration of SANMA was kept constant in SAN. Thus the SANMA concentration of each blend varied with its SAN content.

The same blends were also used for rheological investigations, see Ref. [18]. The results of the morphological analysis (reduction of mean size of inclusions and reduction of coalescence of drops in the compatibilized blend) and the rheological data (linear viscoelastic shear oscillations) clearly indicate that a compatibilization reaction has taken place.

Mechanical characterization

Samples for mechanical testing were shaped according to the ISO 527-2/1BA standard. Measurements in the so-called dry state were performed after drying the specimens for 7 days at 80°C in the vacuum and annealing for 1 h at 90°C in a nitrogen atmosphere. The crosshead velocity of the tensile testing machine was 1 mm/min for the determination of the tensile modulus *E* and 5 mm/min for the measurement of nominal maximum stress σ_{max}, the yield stress σ_{yield}, and elongation at break ε_{break}. All tests were performed at standard climate conditions (23°C, 50% relative humidity).

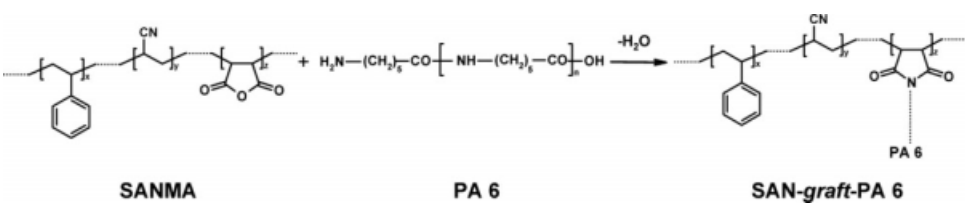

Figure 1 Formation of the compatibilizer by chemical reaction of amino end groups of PA 6 and maleic anhydride entities of SANMA.

Morphological analysis

Specimens for morphological investigations were prepared using an ultramicrotome. First, compression-molded plates were cut into small pieces with approximate dimensions of 10 × 4 × 4 mm^3. Then flat surfaces of the cut specimens were trimmed by means of a diamond knife. For staining, samples of blends were immersed in an osmium/formalin solution for 1 week at a temperature of 60°C. Thereafter, the specimens were dried at 60°C for 3 days. Finally, 85-nm thick thin sections of the samples were cut by microtoming at room temperature with a 35° diamond knife. TEM investigations were performed after transferring the ultrathin sections into the specimen holder of the equipment. The microscope, Leo 912 TEM (Zeiss, Oberkochen, Germany) was operated at an acceleration voltage of 120 kV in the zero-loss-electron mode.

Micromechanical analysis

In situ investigations allow the determination of the micromechanical deformation mechanisms in polymer blends under uniaxial loading.[22] In this study, micromechanical investigations were performed using semithin sections ~ 1-μm thick, several millimeters long, and 0.5-mm wide sliced with an ultramicrotome. These specimens were mounted onto a special microtensile stage specially designed to be used in TEM. Since the mechanical behavior of PA 6 is strongly affected by its moisture content, micromechanical investigations were performed on "dry" and "wet" specimens. The "wet" situation was realized by the application of a water droplet onto the semithin section before the *in situ*-tensile test was run. The time for water absorption was large enough to change significantly the mechanical properties of the PA 6 phase. Assuming the value $D = 10^{-9}$ cm^2/s for the diffusion coefficient D,[23] a complete saturation is obtained after several seconds. Then the wet specimen was stretched (while checking the deformation using a light microscope). The prestretched specimen was placed into a transmission electron microscope and the morphology was investigated. Tensile testing of specimens in the dry state was performed in the vacuum of the TEM. Because of the thickness of the specimens, a high-voltage TEM was required. Courteously, we had access to the JEM 4000 FX microscope (JEOL, Tokyo, Japan) of the Max-Planck-Institute of Microstructure Physics in Halle/S. For the current investigations, the microscope was operated at an acceleration voltage of 400 kV. More details on the technique of micromechanical investigations are given in Refs. 24 and 25.

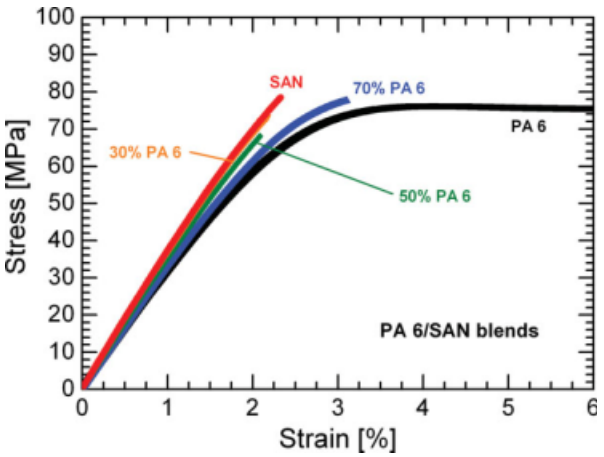

Figure 2 Stress–strain curves (nominal stress σ_{eng} vs. strain ε) at low strains obtained by macroscopic tensile tests on dry samples of PA 6, SAN, and PA 6/SAN blends. [Color figure can be viewed in the online issue, which is available at www.interscience.wiley.com.]

RESULTS

Mechanical experiments

Stress–strain diagrams of the neat blend components and the PA 6/SAN blends are presented in Figure 2. Characteristics taken from the tensile diagrams are summarized in Table II. Before mechanical testing, the materials are dried at elevated temperatures in vacuum and annealed in nitrogen atmosphere. Hence, all mechanical data refer to the so-called dry state of the materials. The stress–strain curve of SAN increases almost linearly with strain until the sample fails because of brittle fracture. Dried PA 6 proved to be much more ductile. Its yield stress equals the maximum stress of SAN, but the elongation at break is 100 times larger, cf. Table II. All PA 6/SAN blends break brittle at nearly the same stress and at low elongations at break (between 2 and 4%). It should be mentioned that PA 6 behaves relatively brittle in the "dry" state, but ductile in the "wet" state (increased moisture content). Water taken up by PA 6 enables the activation of secondary relaxations and thus acts as plasticiser.

Figure 3(a–c) present the tensile modulus E, the maximum stress σ_{max}, the yield stress σ_{yield} for neat PA 6, and the elongation at break ε_{break} of all materials of this study. The Young's modulus of SAN is larger than the modulus of PA 6 [Fig. 3(a)]. An increasing content of PA 6 decreased the modulus of the blends. The variation of modulus with blend composition can be reproduced fairly well by a rule of mixture

$$E_{blend} = \Phi E_{PA\,6} + (1 - \Phi) E_{SAN} \quad (1)$$

where indices refer to the blend and its components and Φ denotes the volume fraction of PA 6 phase.

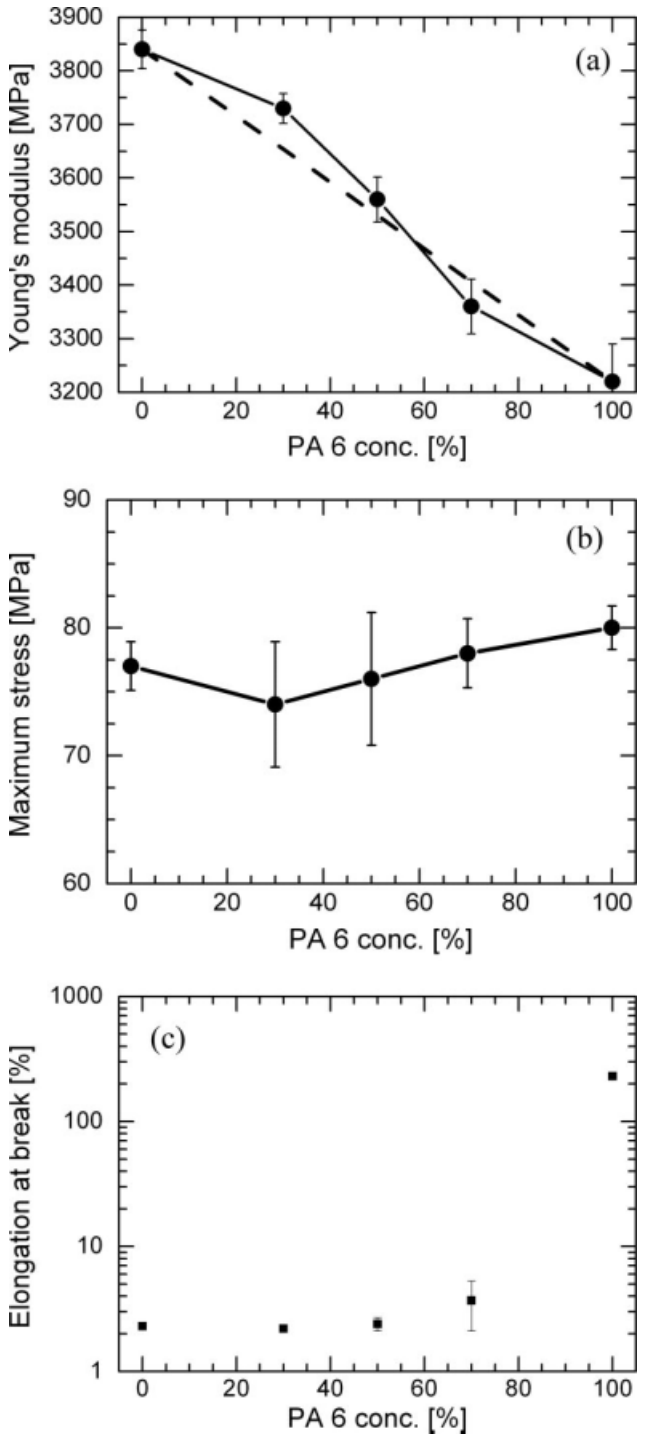

Figure 3 Mechanical properties vs. composition of neat components and PA 6/SAN blends at room temperature. (a) Young's modulus E, (b) maximum stress σ_{max} or yield stress σ_{yield} (for neat PA 6), and (c) strain at break ε_{break}. The dashed line in (a) is calculated from the rule of mixture assumed for E_{blend}, see eq. (1).

Moduli calculated by eq. (1) are drawn as dashed line in Figure 3(a). Small deviations from the rule of mixture seem to occur at concentrations of 30 wt % of SAN and PA 6, respectively. The maximum stress which the materials are capable of bearing seems to increase weakly with PA 6 content [Fig. 3(b)]. Since the standard deviation of the measured data is large compared with their variation due to blend composition an assessment of the impact of composition on σ_{max} becomes virtually impossible. All PA 6/SAN blends break at a low value of elongation [Fig. 3(c)]. Even if PA 6 forms the continuous phase (matrix), the elongation ε_{break} at break remains small (i.e., 3.7%) which is much smaller than the corresponding value of elongation at break of neat PA 6 (ca. 230%). Probably, the interface between PA 6 and SAN phases cannot withstand large deformations and stresses.

Morphological investigations

The microstructure of the different, undeformed PA 6/SAN blends is depicted in Figures 4–7. PA 6 and SAN are immiscible polymers and thus a two-phase morphology is formed. In the TEM micrographs of Figures 5 and 6, the SAN phase appears bright gray and structureless and the PA 6 phase dark gray. Therefore, a clear differentiation of the two polymer phases is rendered possible. The faint streak-like structure to be observed in stained thin sections of neat PA 6 arises from lamellae being typical for the morphology of semicrystalline polymers (Fig. 4). On larger scales, lamellae form the well-known spherolithical structure of PA 6.

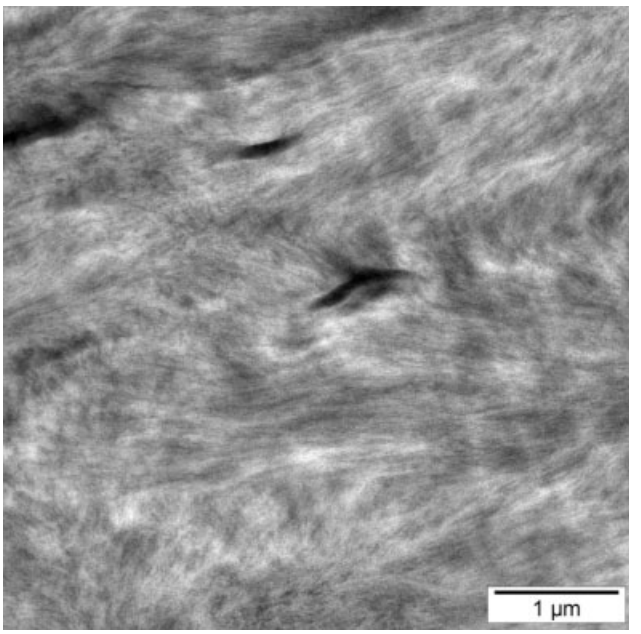

Figure 4 Transmission electron micrographs of neat PA 6 stained with osmium tetroxide. The faint streak-like structures arise from lamellae being typical for the morphology of semicrystalline polymers.

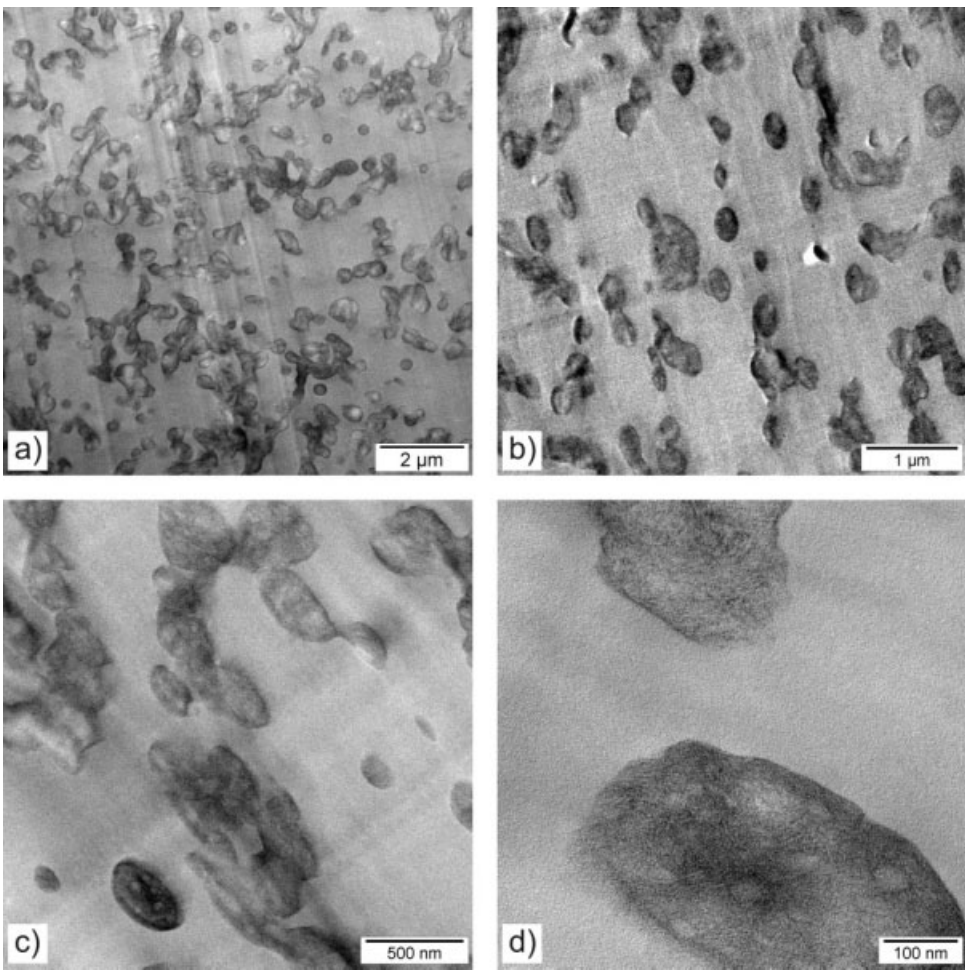

Figure 5 Phase morphology of a selectively chemically stained ultrathin section of the 30% PA 6/70% SAN blend at different magnifications (a–d). The dark phase is PA 6 and the bright phase SAN.

The 30% PA 6/70% SAN blend consists of PA 6 particles which are dispersed in the continuous SAN matrix, cf. Figure 5. The average diameter of the PA 6 particles ranges from 0.2 μm up to 0.5 μm [Fig. 5(b,c)]. Individual PA 6 particles frequently form clusters up to a few micrometers in size. However, the interface between adjacent particles remains visible suggesting that these particles do not merge. The existence of clusters of PA 6 particles demonstrates that agglomeration is not completely prohibited by reactive compatibilization. At a closer look, the PA 6 particles exhibit a substructure composed of tiny SAN or SANMA domains up to 50 nm in size [Fig. 5(d)]. These inclusions are dispersed and stable in the PA 6 phase, i.e., they do not coalesce.

Figure 7 depicts the micrographs of the 70% PA 6/30 % SAN blend. Here, again the continuous phase is constituted by the major component (PA 6) and the uniformly dispersed phase by the minor component (SAN). The size of the SAN particles ranges from 0.1 μm up to 1 μm.

Micromechanical deformation analysis in TEM

30% PA 6/70% SAN and 70% PA 6/30% SAN are blends with one single continuous phase each made up by SAN and PA 6, respectively. Micromechanical tensile tests were performed using semithin sections of these materials. Deformed specimens were subsequently investigated by high-voltage transmission electron microscopy to reveal local deformation mechanisms. Since moisture impairs ductility of the PA 6 component, dried as well as wetted specimens were subjected to tensile tests.

Figures 8 and 9 present the results of the *in situ*-tensile tests. TEM micrographs of dried 30% PA 6/70% SAN blends show very localized deformation zones which occur presumably at structural (e.g., variations in thickness), morphological (e.g., irregularities in the dispersed phase), or compositional (e.g., contaminations) faults within the specimen [near the center part of Fig. 8(c)] or quite obviously ahead of mechanical damages like crack tips

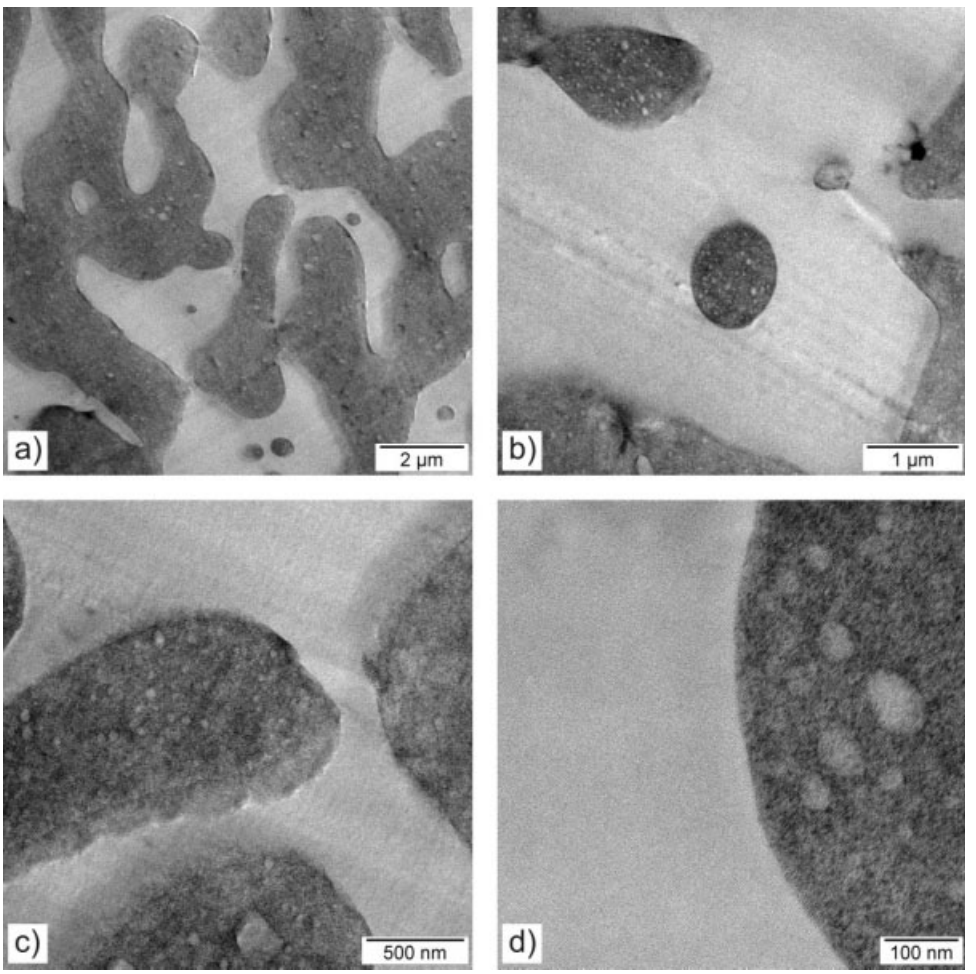

Figure 6 TEM micrographs showing the phase morphology of a selectively chemically stained ultrathin section of the 50% PA 6/50% SAN blend at different magnifications (a–d).

[upper left Fig. 8(c)]. Having been brought into contact with water, which enables PA 6 to become ductile, the deformation pattern changes from inhomogeneous localized crazing to homogenous multiple crazing [Fig. 8(a, b)]. The pattern now appears alike deformation structures being observed in rubber-modified polystyrene (high impact polystyrene, HIPS) and rubber-modified SAN (ABS with about 0.5-µm wide rubber particles), where crazes, fibrillated, and completely yielded deformation zones, are initiated by rubber particles, which were forced to cavitate by negative pressure stress fields.[26] The crazes [visible as short bright streaks in Fig. 8 (a,b)] are aligned along deformation bands tilted by about $\pm 75^\circ$ to the tensile axes. This implies that shear deformation also plays a certain role although crazing is the dominant deformation process.

Tensile deformation of wetted blends of the inverse composition, 70% PA 6/30% SAN, is characterized by the appearance of broad bands of highly stretched material [Fig. 9(a)]. With respect to the tensile axes, initially crazing occurs at the poles of SAN particles which were typically 500 nm wide. The initiating step for crazing might be partial failure of the PA 6/SAN interface. Eventually, at sufficiently high deformations fibrils of crazes fail leaving SAN particles completely debonded at one of the two poles. The void which was formed continuously deforms into an elliptically shaped hole by shear yielding of the surrounding matrix as long as the tensile stress is maintained. Thus, rigid SAN particles are always to find at one side of the void [Fig. 9 (b)]. Finally, wide deformation zones with high-local extension ratios of about 4 are formed. These bands are separated by regions wherein deformation stays small. Sometimes small SAN particles are found well imbedded into strands of elongated PA 6. The size of these particles, which seem not to disturb the deformation of the matrix is of the order of the thickness of elongated ligaments.

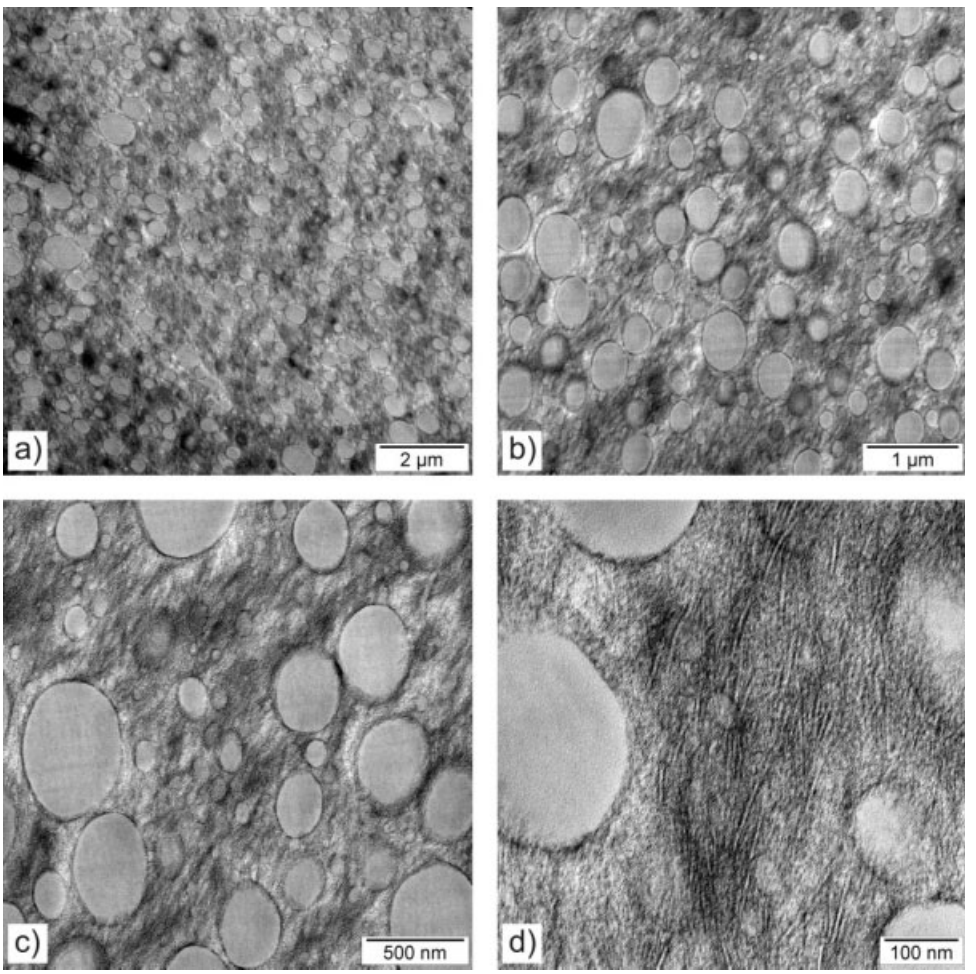

Figure 7 Phase morphology (transmission electron micrograph) of a stained ultrathin section of the 70% PA 6/30% SAN blend at different magnifications (a–d).

DISCUSSION

The morphology of PA 6/SAN blends was strongly influenced by the blend composition. Equal amounts of PA 6 and SAN (50%/50%) led to an interpenetrating network after compression molding. In unbalanced compositions, the majority component made up the continuous matrix phase and the minority component the dispersed, particle-like phase. In PA 6 phases generally small inclusions were found, which were attributed to SAN and/or SANMA. Some of the SANMA compatibilizer seems to be located at the interface between SAN particles and PA 6 matrix. These compatibilizer molecules, which should mechanically interlink the different polymer phases, showed microfibrillation at least during mechanical loading of blends with a PA 6 matrix. The dispersed SAN particles behaved like rigid spheres. After rupture of fibrils, thin strands of matrix polymer, which separated the SAN particles, were capable of deforming plastically up to large extension ratios. In blends with SAN matrices, the PA 6 to SANMA ratio was increased and the dispersed PA 6 particles seemed to be well bonded to the surrounding matrix. This prompted a ductile behavior, i.e., moist PA 6 particles to behave like rubber particles tightly bonded to a rigid matrix by grafting. Thus, homogeneous microcrazing was initiated accompanied by some shear deformation of the matrix.

Macroscopic mechanical tests accomplished at dried specimens showed increasing Young's moduli with increasing SAN contents. All other data like maximum stress, yield stress, and elongation at break did not change much with blend composition. All of the blends containing SAN behaved brittle. These results correlate with data of micromechanical tests at blends in the dry state. Tensile tests performed at wetted blends, however, revealed a high ductility. In wetted blends, the disperse phase (minority phase) caused stress concentration and initiated plastic deformation of the

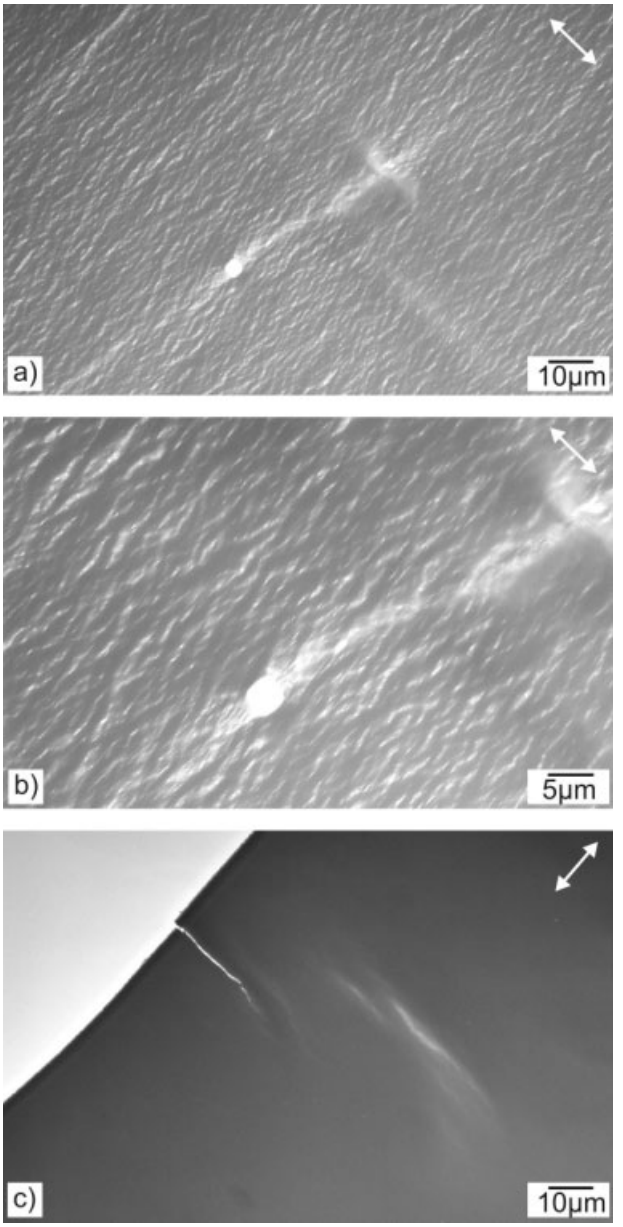

Figure 8 TEM micrograph of semithin sections (1 µm thick) of 30% PA 6/70% SAN after tensile deformation. The double arrow indicates the tensile direction. (a,b) Homogeneous deformation due to multiple crazing and partial shear deformation to be found in wetted specimens. Shear bands are tilted by about ±75° with respect to the tensile axis. (c) Crazing ahead of a crack tip (upper left) and localized crazing inside a dried specimen (center part). The bright cushion-like distorted spot in (a) and (b) arises from a hole in the sample.

matrix – predominantly crazing in SAN and shear yielding in PA 6. Moist PA 6 particles turned out to be weak enough to act as stress concentrators and were apparently able to reduce the triaxial stress field by presumably some kind of cavitation hence initiating crazing in their vicinity. On the other hand, with stiff SAN particles, shear yielding is initiated after debonding. These observations correlate very well with the results for PA 6/ABS blends and show that the addition of 10 wt % of rubber particles did neither modify phase morphology nor change micromechanical properties. Intense plastic deformation—either crazing or shear yielding—of matrix strands between adjacent cavitated particles or voids absorbs energy. Therefore, a higher ductility with larger elongation at break will also be expected for macroscopic mechanical tests if accomplished using moist samples.

In 70% PA 6/30% SAN blends debonding appeared only around SAN particles with diameters larger than about 200 nm. No debonding was

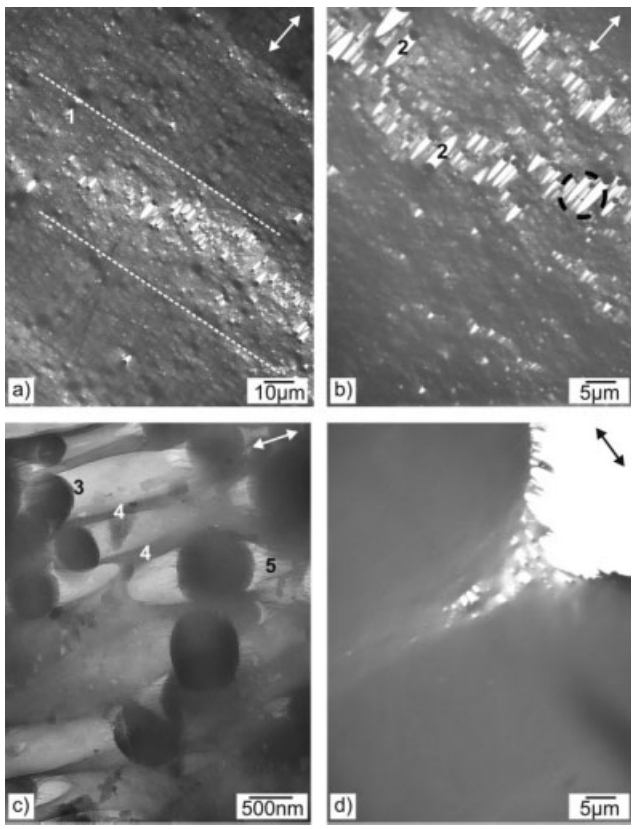

Figure 9 Deformation in wetted (a–c) and dried (d) specimens of 70% PA 6/ 30% SAN blends. TEM micrographs reveal the processes involved in deformation: partial failure of PA 6/SAN interfaces and fibrillation at the poles of SAN particles (dark spheres with a diameter of ca. 500 nm), formation of microvoids by rupture of fibrils at one of the pole, elongation of microvoids by shear yielding of thin matrix strands. Large deformation occurs in broad bands separated by bands of weakly deformed material. Small particles imbedded into matrix ligaments seem not to disturb their deformation [highlighted by a circle in (b)]. In the case of dried specimens, these processes are restricted to small volumes ahead of crack tips where stress concentration takes place. Hence, dried specimens behave relatively brittle compared with wetted ones. The numbers denote: 1 deformation band, 2 void, 3 pole, 4 elongated PA 6 strand, and 5 fibrilles.

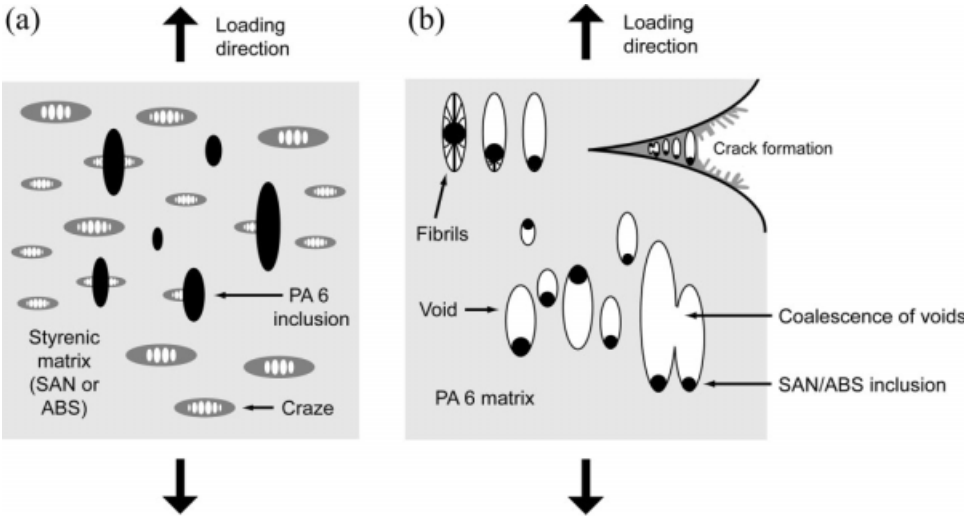

Figure 10 Scheme of deformation mechanisms in PA 6/SAN and PA 6/ABS blends (wet state). (a) Moist and consequently soft PA 6 inclusions promote crazing in the less ductile SAN or ABS matrix. The sketch illustrates craze formation at an early stage of deformation. For simplification, shear yielding is not taken into account. (b) The deformation in the vicinity of rigid inclusions of SAN or ABS starts out with voiding at the poles of particles accompanied by fibrillation of the interface between particle and matrix and is followed by partial debonding of particles and elongation of the holes formed.

observed around SAN particles smaller than about 100 nm. If we assume that the surface concentration of SAN-*graft*-PA 6 molecules on the SAN particles does not depend on the particle size, this observation might qualitatively be explained by fundamental fracture mechanics: the smaller the size of a flaw the higher the failure stress. Thus below a certain critical diameter, the failure stress exceeds the yield stress of the matrix and the flaw no longer initiate failure. In consequence at tensile loading, the matrix will preferentially fail at the largest SAN particles. After failure—crazing of or debonding at the interface—the triaxial stress field is locally reduced and the material starts flowing. The stress field around small particles that are imbedded in the deforming ligaments are now by far too small to cause interfacial failure.

Figure 10 summarizes the experimental findings for the blends in the wet state in a scheme. The deformation of (moist) PA 6 particles in a styrenic matrix (SAN or ABS) yields uniform crazing [Fig. 10(a)]. If (rigid) SAN particles form inclusions in the matrix of PA 6, then the interface is strongly deformed which leads to the formation of fibrils and voids, respectively. The SAN particles are not significantly elongated. If several voids coalesce, a macroscopic crack is formed [Fig. 10(b)].

Small inclusions of rigid polymer particles imbedded in the matrix of a slightly softer polymer are prone to deform plastically at least if an adequate difference between both moduli and Poisson's ratios, which should be lower for the disperse phase, exists.[27–29] Further prerequisites for this phenomenon called inclusion yielding are deemed to be a sufficiently fine phase morphology and a high interfacial adhesion. For compatibilized and moist PA 6/SAN blends with 30% and 70% of SAN concentration, a morphology was observed that could have fit these demands: small rigid SAN particles are dispersed in softer particles of PA 6 or in a softer matrix of PA 6. Nevertheless in none of the microtensile tests performed at wetted specimens, there was evidence for inclusion yielding. The reason is speculative. They can likewise be found in inadequate mechanical constants or weak bonding of the rigid particles to their environment which might prohibit stress to rise to a critical value to initiate shear yielding.

CONCLUSIONS

In this study (Part II), morphological and mechanical properties of reactively compatibilized PA 6/SAN blends were investigated and compared with those of PA 6/ABS blends which were reported in Part I. Micromechanical deformation processes were studied by performing *in situ*-tensile tests at semithin sections in a TEM. Since mechanical properties of PA 6 strongly depend on moisture content, the experiments were accomplished at "dried" and "wetted" specimens. The experimental results yield the following conclusions:

1. The development of the morphology of SANMA modified PA 6/SAN blends follows a scheme typical for an effective compatibilization: it starts

out with SAN matrices and imbedded spherical PA 6 particles at low PA 6 contents, traverses cocontinuous networks at about equal amounts of both constituents and eventually undergoes phase inversion. Dispersed PA 6 particles are never found neat but always contained small micelle-like inclusions of SAN or SANMA. The morphological changes are very similar to the results for PA 6/ABS blends (Part I).
2. Blends in the "dry" state behave much more brittle than in the "wet" state. Moist PA 6 particles and matrices are sufficiently ductile to initiate homogeneous crazing in SAN matrices and to large elongations in thin unconstrained ligaments being created by debonding of SAN particles, respectively.
3. The compatibilizer SANMA forms small domains in PA 6 particles and makes up the interface between PA 6 and SAN domains.
4. In blends with a ductile matrix and rigid particles (70% PA 6/30% SAN), local failure is initiated by rupture and crazing of the interface between the constituents. This observation is very similar to what was found in PA 6/ABS blends.

The authors are very thankful to W. Schmidheiny, F. Mettler, and J. Hostettler for the support of the experimental work. The authors express their gratitude to Prof. Dr. U. Gösele (Max Planck Institute of Microstructure Physics) for the possibility to use the transmission electron microscope. Mechanical experiments were performed within the IUPAC Subcommittee "Structure and Properties of Commercial Polymers" (# 2005-023-2-400).

References

1. Utracki, L. A. Commercial Polymer Blends; Chapman and Hall: London, 1998.
2. Weber, M. Macromol Symp 2001, 163, 235.
3. Weber, M. Macromol Symp 2002, 181, 189.
4. Weber, M.; Heckmann, W.; Goeldel, A. Macromol Symp 2006, 233, 1.
5. Van Duin, M.; Machado, A. V.; Covas, J. Macromol Symp 2001, 170, 29.
6. Handge, U. A.; Sailer, C.; Steininger, H.; Weber, M.; Scholtyssek, St.; Seydewitz, V.; Michler, G. H. J Appl Polym Sci 2009, 112, 1658.
7. Jafari, S. H.; Pötschke, P.; Stephan, M.; Warth, H.; Alberts, H. Polymer 2002, 43, 6985.
8. Jafari, S. H.; Pötschke, P.; Stephan, M.; Pompe, G.; Warth, H.; Alberts, H. J Appl Polym Sci 2002, 84, 2753.
9. Lee, C. W.; Ryu, S. H.; Kim, H. S. J Appl Polym Sci 1997, 64, 1595.
10. Pötschke, P.; Paul, D. R. Macromol Symp 2003, 198, 69.
11. Takeda, Y.; Paul, D. R. J Polym Sci Part B: Polym Phys 1992, 30, 1273.
12. Majumdar, B.; Paul, D. R.; Oshinski, A. J. Polymer 1997, 38, 1787.
13. Majumdar, B.; Keskkula, H.; Paul, D. R. J Polym Sci Part B: Polym Phys 1994, 32, 2127.
14. Majumdar, B.; Keskkula, H.; Paul, D. R. Polymer 1994, 35, 5453.
15. Kudva, R. A.; Keskkula, H.; Paul, D. R. Polymer 2000, 41, 225.
16. Kitayama, N.; Keskkula, H.; Paul, D. R. Polymer 2001, 42, 3751.
17. Araújo, E. M.; Hage, E., Jr.; Carvalho, A. J. F. J Appl Polym Sci 2003, 90, 2643.
18. Sailer, C.; Handge, U. A. Macromolecules 2007, 40, 2019.
19. Sailer, C.; Handge, U. A. Macromol Symp 2007, 254, 217.
20. Sailer, C.; Handge, U. A. Macromolecules 2008, 41, 4258.
21. Sailer, C.; Weber, M.; Steininger, H.; Handge, U. A. Rheol Acta 2009, 48, 579.
22. Altstädt, V.; De Lucca Freitas, L.; Schubert, D. W. Pure Appl Chem 2004, 76, 389.
23. Hanspach, J.; Pinno, F. Acta Polym 1992, 43, 210.
24. Michler, G. H.; Lebek, W. Ultramikrotomie in der Materialforschung; Carl Hanser Publishers: München, 2004.
25. Michler, G. H. Electron Microscopy of Polymers; Springer: Berlin, 2008.
26. Kambour, R. P. J Polym Sci Part D: Macromol Rev 1973, 7, 1.
27. Michler, G. H. In Mechanical Properties of Polymers Based on Nanostructure and Morphology; Michler, G. H., Baltá-Calleja, F. J., Eds.; Taylor and Francis: Boca Raton, 2005; p 379–432.
28. Kolarik, J.; Lednicky, F.; Locati, G.; Fambri, L. Polym Eng Sci 1997, 37, 128.
29. Kelnar, I.; Stephan, M.; Jakisch, L.; Fortelný, I. J Appl Polym Sci 1999, 74, 1404.